Surface Convergence Induced by Cold Fronts Aloft and Prefrontal Surges

JOHN D. LOCATELLI, MARK T. STOELINGA, RALPH D. SCHWARTZ, AND PETER V. HOBBS

Atmospheric Sciences Department, University of Washington, Seattle, Washington

(Manuscript received 10 May 1996, in final form 6 March 1997)

ABSTRACT

The magnitude of surface convergence, produced by the movement of cold fronts aloft and prefrontal surges, is derived by applying the linear divergence equation to observed surface pressure traces for Pacific Northwest warm occlusions and from a mesoscale model simulation of a warm occlusion–like structure in the central United States. Convergence values of approximately 10^{-4} s^{-1} are found to be generated locally for periods of about 1 h, yielding vertical displacements of 10–50 hPa. It is hypothesized that such convergences should noticeably enhance condensation rates in the widespread lower stratiform clouds associated with warm occlusions and could be a key mechanism for the triggering of squall lines by cold fronts aloft in cyclones in the central United States.

1. Introduction

It has been well documented that the passage of a cold front aloft (CFA) within a warm-type occlusion is associated with short-term pressure changes at the surface. Holzman (1936) concluded that the passage of an upper cold front is usually characterized by ''a slower rate of [pressure] decrease or only a slight rise in the barometer.'' Lichtblau (1936) noted that the ''surface isobars along the cold front aloft will show a trough with no sharp discontinuities at the front'' and that ''pressure tendencies afford the best clue for the recognition and the determination of the progress of the cold front aloft.'' These observations were verified by Wexler (1935), Williams (1953), Galloway (1958), Locatelli et al. (1982), and Matkovskii and Shakina (1982). In addition to a CFA, warm occlusions often contain one or more prefrontal surges, which are structurally similar to a CFA (Kreitzberg and Brown 1970; Matejka et al. 1980), but occur prior to the passage of the ''final'' CFA over the warm front. Matejka et al. (1980) noted that the passage overhead of a prefrontal surge rainband is also marked on a barogram by a temporary slight rise in the pressure or a lessening in the rate of pressure fall.

Of particular interest is the possibility that the local change in the surface horizontal pressure gradient associated with the passage of a CFA produces surface convergence that is locally of sufficient magnitude and duration to cause significant vertical displacement of low-level air parcels. We will refer to this phenomenon as *CFA-induced surface convergence.* Showalter and Fulks (1943) determined that ''regions most conducive to convergence [at the surface] are those just in advance of a surface or upper [cold] front.'' Matejka (1980) postulated that surface convergence induced by CFAs enhances precipitation in classic warm occlusions, such as those studied during the Cyclonic Extratropical Storms (CYCLES) project in the Pacific Northwest. Locatelli et al. (1995) postulated that CFA-induced surface convergence might be sufficient to trigger vigorous line convection in the warm-occluded-like structures observed in winter and spring cyclones in the central United States. In the Structurally Transformed by Orography Model (STORM), described by Hobbs et al. (1996), a trough in the lee of the Rocky Mountains often marks the surface position of a weak frontal zone that slopes upward to the east or northeast; this resembles a classic warm front, but the frontal zone is characterized by significant convective instability. This feature has been termed a *drytrough* (Martin et al. 1995). The occlusion of this warm-frontal-like structure by a CFA is often accompanied by a convective rainband that is more closely aligned with the leading edge of cold advection aloft than it is with the drytrough or any other surface features. Locatelli et al. (1995) used a simple numerical model to calculate the convergence due to the differential accelerations of air parcels located beneath the nose of a CFA that occluded a convectively unstable drytrough structure in the central United States on 9 March 1992. These calculations yielded vertical velocities on the order of tens of centimeters per second.

The structure, distribution of precipitation, and dynamic evolution of winter and spring cyclones in the central United States is a complex phenomenon involv-

Corresponding author address: Dr. Peter V. Hobbs, Department of Atmospheric Sciences, University of Washington, Box 351640, Seattle, WA 98195-1640.
E-mail: phobbs@atmos.washington.edu

ing synoptic-scale (quasigeostrophic) dynamics, terrain interactions, mesoscale dynamics, and cloud microphysical processes. However, the present study focuses on a specific question related to warm-occluded-like structures in general, namely, what is the immediate effect (within about 1 h) of a well-defined, leading edge of cold advection aloft, which moves relative to surface air parcels, on low-level pressure changes, convergence, and vertical air velocity? The purpose of this study is to develop a simple mathematical relationship that aids understanding and quantifies CFA-induced surface convergence, and then to apply this relationship to several well-documented cases of warm-occluded-like structures. While it is proposed that CFA-induced surface convergence can trigger and maintain convective CFA rainbands (as depicted in the STORM conceptual model), it is desirable to study first the effect on convergence of a migratory CFA when convection is not involved. This is because, in the absence of strong diabatic heating or cooling and nonhydrostatic pressure perturbations associated with vigorous convection, the surface pressure pattern associated with the passage of a CFA can be more readily extracted from the data. Therefore, the cases chosen for this study are warm-occluded-like structures that involve stably stratified warm fronts and stratiform precipitation. The results of this study pertain specifically to the possible enhancement of stratiform precipitation within stably stratified warm occlusions and, by inference, to the possible release of convective instability in unstably stratified warm-occluded-like structures.

Since the surface convergence induced by the passage of a CFA is associated with a measurable change in the surface horizontal pressure gradient, one might appeal to the concept of the quasigeostrophic isallobaric wind to quantify it. In quasigeostrophic theory, it is assumed that an ageostrophic wind accompanies a Lagrangian change in the horizontal pressure gradient, such that the Coriolis effect acting on the ageostrophic wind exactly balances the acceleration of the geostrophic wind defined by the changing horizontal pressure gradient [see, e.g., Eq. (6.40) in Holton (1992)]. However, this approach is strictly valid only for synoptic-scale, slowly varying, pressure patterns. For example, the application of Holton's Eq. (6.40) to the abrupt pressure tendency changes seen in barograms as a CFA passes overhead, yields ageostrophic winds of hundreds of meters per second! Another approach to the quantification of the surface convergence produced by a CFA would be to include the effect of friction and assume geotriptic balance, which is a balance between the horizontal pressure gradient, Coriolis, and friction forces (Johnson 1966). The change in horizontal pressure gradient that accompanies the CFA would result in frictional convergence, as suggested by Matejka (1980). However, this approach also requires a balance assumption, which is not met until several hours after the abrupt pressure changes associated with the passage of a CFA.

The approach that we will take here is to quantify the CFA-induced surface convergence with the simplest possible equation that does not assume balance, but rather allows parcels to be accelerated by the *imbalance* of forces. We present first an approximate solution that utilizes a form of the linear divergence equation, the use of which is justified in section 2. We then present results of an application of this equation to two warm occlusions observed in the Pacific Northwest (section 3). In section 4, the occlusion of an arctic front in the central United States is examined by means of a mesoscale model simulation, and the vertical displacements of parcels obtained from the model are compared to those predicted by the linear divergence equation. The paper concludes (in section 5) with a discussion of the results of this study.

2. The linear divergence equation and its application to barograms

Figure 1a shows a schematic vertical cross section through a warm occlusion with a CFA moving over the warm-frontal zone. For simplicity, the x axis is shown parallel to the gradients of potential temperature in both the warm- and cold-frontal portions of the occlusion. The CFA moves in the positive x direction at a speed S relative to the ground, which is generally faster than the velocity (in the positive x direction) of the air below the warm front. Therefore, the CFA passes over low-level air parcels. The resulting surface pressure field is divided into two parts. The background (pre-CFA) state is characterized by geotriptic balance in which the horizontal gradient of the background pressure ($\overline{p}$) is uniform; therefore, the background state is characterized by a horizontally uniform nondivergent wind field (Fig. 1b). It should be noted, however, that the gradient of $\overline{p}$ need not be oriented along the x axis (as shown in Fig. 1b); that the background wind field in the x direction, $\overline{u}$, may be nonzero; and that $\overline{u}$ may have a nonzero vertical shear. The perturbation pressure field at the surface (p', shown in Fig. 1c) is associated with the moving CFA (the region within the dotted box in Figs. 1a,c). We will assume that the CFA, which induces p', has a structure that is unchanging during the time period of interest (about 1 h). Therefore, the local tendency of p', and the horizontal gradient of p', can be obtained from each other by means of a space-to-time conversion. As the moving pressure perturbation (Fig. 1c) overtakes low-level air parcels, acceleration of the perturbation velocity in the x direction commences at different times for neighboring parcels. These differential velocities result in a moving pattern of convergence and vertical velocity at low levels, as depicted schematically in Fig. 1d. The goal of this section is to quantify the expected convergence and ascent for low-level parcels above an observing station over which a CFA passes, based on the barogram pressure trace (i.e., the time evolution of p') at that station.

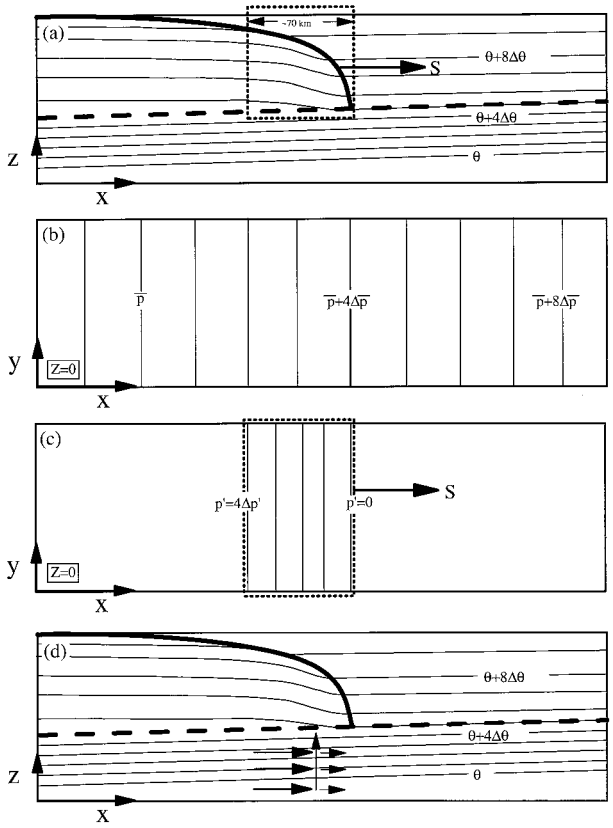

FIG. 1. (a) Schematic vertical cross section of the pattern associated with a warm occlusion. The top of the warm front is marked by the heavy dashed line, and the cold front aloft (CFA) by the heavy solid line. The arrow indicates the direction of movement of the CFA, which is moving at speed *S*. The dashed box encloses the portion of the potential temperature field that causes the moving perturbation pressure pattern shown in (c). (b) Plan view of the base state surface pressure pattern where geotriptic balance is maintained. (c) Plan view of the perturbation pressure pattern at the surface. The arrow indicates the direction of movement of the perturbation in the surface pressure pattern, which moves at speed *S*. (d) Schematic vertical cross section showing the different perturbation horizontal speeds (horizontal arrows) of air parcels in the boundary layer below the moving CFA caused by the moving perturbation pressure pattern, and the resulting vertical air velocity (vertical arrow).

Due to the two-dimensionality of the situation depicted in Fig. 1, the convergence can be analyzed with the x momentum equation:

$$\frac{\partial u}{\partial t} = -u\frac{\partial u}{\partial x} - w\frac{\partial u}{\partial z} - \rho^{-1}\frac{\partial p}{\partial x} + fv - ku, \quad (1)$$

where u, v, and w are the velocities in the x, y, and z directions, respectively; ρ is air density; p is pressure; f is the Coriolis parameter; and k is the linear coefficient for a Rayleigh-type representation of friction. Taking the partial derivative of (1) with respect to x, assuming that horizontal density variations are small, and noting that convergence (c) is equal to $-\partial u/\partial x$, we obtain

$$\frac{\partial c}{\partial t} = -u\frac{\partial c}{\partial x} + c^2 - w\frac{\partial c}{\partial z} + \frac{\partial w}{\partial x}\frac{\partial u}{\partial z} + \rho^{-1}\frac{\partial^2 p}{\partial x^2} - f\frac{\partial v}{\partial x} - kc. \quad (2)$$

Substituting the background and perturbation quantities into (2), and noting that $\overline{c} = 0$ due to the uniform horizontal pressure gradient in the background state, the following equation for the perturbation convergence at low levels (c') is obtained:

$$\frac{\partial c'}{\partial t} = -\overline{u}\frac{\partial c'}{\partial x} - u'\frac{\partial c'}{\partial x} + c'^2 - w'\frac{\partial c'}{\partial z} + \frac{\partial w'}{\partial x}\frac{\partial \overline{u}}{\partial z} + \frac{\partial w'}{\partial x}\frac{\partial u'}{\partial z} + \rho^{-1}\frac{\partial^2 p'}{\partial x^2} - f\frac{\partial v'}{\partial x} - kc'. \quad (3)$$

To simplify (3) we can perform a scale analysis on each of the terms. As a CFA (or a prefrontal surge) passes overhead, both $\partial^2 p'/\partial x^2$ and $\partial^2 p'/\partial t^2$ attain large positive values, due to the influx of cold air aloft. The barogram segments displayed in Figs. 3c, 4c, and 4d show this period to last around 20–30 min, so the timescale T is taken to be 10^3 s. Time-to-space conversion of the barogram segments yields a magnitude of around 10^{-7} s^{-2} for the term $\rho^{-1}\partial^2 p'/\partial x^2$ in (3). The ground-relative speed S of the CFA, normal to its orientation, is typically around 20 m s^{-1}. The length scale L is chosen as the distance the CFA, and its associated surface pressure pattern, travel during the timescale, or $L = ST = 2 \times 10^4$ m. Observations by Matejka (1980) indicate that surface winds undergo changes in velocity of only a few meters per second during the passage of a CFA or a prefrontal surge, so the u velocity is scaled as $U = 2$ m s^{-1}. The convergence is scaled as $C = U/L = 10^{-4}$ s^{-1}. The scale for v' can be estimated by the Coriolis effect ($f = 10^{-4}$ s^{-1}) acting on u' as it increases from zero to U during the period T, which can be estimated as $V = fUT = fCST^2 = 0.2$ m s^{-1}. The scale for $\overline{u}$ is taken to be $\overline{U} = 20$ m s^{-1}, which is consistent with the most extreme example (in terms of $\overline{u}$) considered in this paper. The choice for a scale height H is arbitrary, because it is simply the height at which one wishes to determine the induced vertical velocity and net vertical displacement resulting from this phenomenon, but is subject to the limitation that it should not approach the height of the CFA. It is taken to be 1 km. The scale for w' at the top of this layer is estimated as $W = CH = 10^{-1}$ m s^{-1}. Finally, the value of k is liberally estimated as (3 h)$^{-1}$, or approximately 10^{-4} s^{-1}. With these assumptions, the scales of all the terms in (3) can be estimated. The values are given in Table 1. Retaining the four terms that are of order 10^{-7} s^{-2}, the following equation is obtained:

$$\frac{\partial c'}{\partial t} = -\overline{u}\frac{\partial c'}{\partial x} + \frac{\partial w'}{\partial x}\frac{\partial \overline{u}}{\partial z} + \rho^{-1}\frac{\partial^2 p'}{\partial x^2}. \quad (4)$$

Equation (4) is similar to the linear divergence equation

TABLE 1. Estimated order of magnitude of the terms in Eq. (3). See text for explanation.

Term	Scale definition	Scale value (s^{-2})
$\frac{\partial c'}{\partial t}$	$\frac{C}{T}$	10^{-7}
$-\overline{u}\frac{\partial c'}{\partial x}$	$\overline{U}\frac{C}{L}$	10^{-7}
$-u'\frac{\partial c'}{\partial x}$	$U\frac{C}{L}$	10^{-8}
c'^2	C^2	10^{-8}
$-w'\frac{\partial c'}{\partial z}$	$W\frac{C}{H}$	10^{-8}
$\frac{\partial w'}{\partial x}\frac{\partial \overline{u}}{\partial z}$	$\frac{W}{L}\frac{\overline{U}}{H}$	10^{-7}
$\frac{\partial w'}{\partial x}\frac{\partial u'}{\partial z}$	$\frac{W}{L}\frac{U}{H}$	10^{-8}
$\rho^{-1}\frac{\partial^2 p'}{\partial x^2}$	taken from obs. or model	10^{-7}
$-f\frac{\partial v'}{\partial x}$	$f\frac{V}{L}$	10^{-9}
$-kc'$	kC	10^{-8}

that arises in linear gravity wave theory [see, e.g., Eq. (6.4.7) in Gill (1982)], with the addition of two terms arising from a nonzero background velocity. The simplicity of this equation makes it useful in estimating the magnitude of CFA-induced surface convergence. However, it cannot be applied for an arbitrary length of time because, although the scale analysis resulted in the dropping of the Coriolis term in (3), it is clear that geostrophic adjustment will eventually reduce the convergence generated by the abrupt change in pressure gradient associated with the moving CFA. It is conservatively estimated that such an adjustment can be neglected for at least 60 min. Therefore, (4) will be used here only to estimate the effects of the moving CFA only within 60 min of its passage.

To make (4) more useful, the inclusion of a vertically varying $\overline{u}$ must be simplified. The justification for this simplification becomes apparent upon examination of the vertical profiles of $\overline{u}$ for the three CFA cases to be presented in this paper (which will each be described in more detail later). Shown in Fig. 2 are the three vertical profiles of $\overline{u}$ in the lowest 1 km above ground level, which were calculated by taking the component of wind perpendicular to the approaching CFA but several kilometers ahead of the CFA. For the two Pacific Northwest cases, winds were obtained from soundings. For the model-simulated case (section 4), the winds were obtained from model output. Although $\overline{u}$ varies significantly with height in each case, it is also apparent that each profile lends itself to being approximated by two layers of linear shear, separated by a transition height that will be referred to as z. The lower layer will

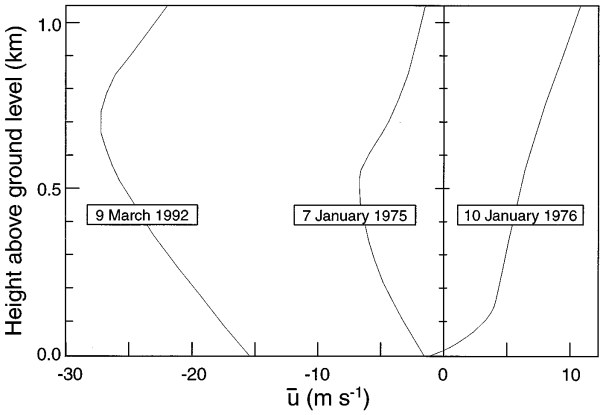

FIG. 2. Vertical profiles of $\overline{u}$, the background velocity in the direction of the CFA movement, prior to the arrival of the CFA. The 7 January 1975 and 10 January 1976 profiles were obtained from soundings, and the 9 March 1992 profile was obtained from numerical model output.

be referred to as layer 1, and the upper as layer 2. The values of $\partial\overline{u}/\partial z$ in each layer will be referred to as $\overline{u}_{z1}$ and $\overline{u}_{z2}$. The values of z_t, $\overline{u}_{z1}$, and $\overline{u}_{z2}$, which are shown in Table 2 for the three cases, will be used in later calculations of convergence and vertical ascent.

We first apply (4) to layer 1, assuming that ρ and p' are approximately independent of height in the lowest 1 km. Under these conditions, we attempt to solve (4) for c_1' (the perturbation convergence in layer 1), assuming it too is independent of height. That assumption cannot be justified a priori but will be validated by the solution obtained. Since we are interested in only the lowest 1 km of the atmosphere, we make use of the incompressible continuity equation, $\nabla\cdot\mathbf{v} = 0$, and we also assume that $w' = 0$ at the ground. Therefore, if c_1' is independent of height, then $w_1' = zc_1'$, and $\partial w_1'/\partial x = z\partial c_1'/\partial x$. Also, in layer 1, the background wind at height z can be written as $\overline{u}(z) = \overline{u}(0) + z\overline{u}_{z1}$. Finally, if the assumption is made that the CFA-induced surface pressure pattern and the associated convergence pattern are fixed structures that move at constant velocity S, the time/space conversion $\partial/\partial t = -S\partial/\partial x$ can be employed. Substituting these relationships into (4), we obtain for layer 1

$$\frac{\partial c_1'}{\partial t} = \frac{1}{\rho S[S - \overline{u}(0)]}\frac{\partial^2 p'}{\partial t^2}. \tag{5}$$

TABLE 2. Parameters for three occlusion cases. See text for explanation.

Case	z_t (m)	$\overline{u}_{z1}$ (s^{-1})	$\overline{u}_{z2}$ (s^{-1})	S(m s^{-1})	$\overline{u}(0)$ (m s^{-1})
10 January 1976	0.15	0.038	0.008	24	−1
7 January 1975*	0.50	−0.011	0.011	13	−1
9 March 1992	0.70	−0.018	0.023	16	−16

* Parameters for the 7 January 1975 case apply to both the prefrontal surge and the CFA.

Note that height z does not appear on the right-hand side of (4), which validates the assumption that c_1' is independent of height in layer 1. Thus, in layer 1, the assumption of linear shear reduces (4) to a simple relationship between the local convergence tendency and the local second time derivative of p', given the constants S and $\overline{u}(0)$. The value of the shear does not appear in (5), due to a cancellation between the vertical velocity term and the shear part of the advection term in (4).

The situation is somewhat more complicated for layer 2. The derivation follows that for layer 1, except in layer 2, $w_2' = z_t c_1' + (z - z_t)c_2'$ and $\overline{u}(z) = \overline{u}(0) + z_t\overline{u}_{z1} + (z - z_t)\overline{u}_{z2}$. Using these relationships, the counterpart for (5) in layer 2 can be derived, namely:

$$\frac{\partial c_2'}{\partial t} = \frac{A}{\rho S[S - \overline{u}(0)]}\frac{\partial^2 p'}{\partial t^2}, \tag{6}$$

where

$$A = \frac{S - \overline{u}(0) - z_t\overline{u}_{z2}}{S - \overline{u}(0) - z_t\overline{u}_{z1}}. \tag{7}$$

If the factor A is less than 1, which occurs when there is a positive change in shear from layer 1 to layer 2, the convergence produced in layer 2 by the passage of the CFA will be reduced from the amount expected for a single layer with constant linear shear throughout.

Equations (5) and (6) can be further manipulated to obtain expressions for the convergence and vertical velocity at a fixed location on the ground as a function of time and height and, ultimately, the net vertical displacement as a function of time and initial height for a low-level parcel over which the CFA passes. First, (5) and (6) must be integrated in time. If the initial time of the integration is defined as just prior to the arrival of the CFA, then the definitions of the background and perturbation convergence and pressure imply that p', $\partial p'/\partial t$, c_1', and c_2' are all zero at $t = 0$. Therefore, time integration of (5) and (6) yields

$$c_1' = \frac{1}{\rho S[S - \overline{u}(0)]}\frac{\partial p'}{\partial t}$$

and (8)

$$c_2' = \frac{A}{\rho S[S - \overline{u}(0)]}\frac{\partial p'}{\partial t}.$$

Since we are more interested in the vertical velocity in the higher layer (layer 2), we make use of the relationship $w_2' = z_t c_1' + (z - z_t)c_2'$, and substitute the convergence expressions in (8), yielding

$$w_2' = \frac{[z_t + A(z - z_t)]}{\rho S[S - \overline{u}(0)]}\frac{\partial p'}{\partial t}. \tag{9}$$

Finally, we seek to quantify the net vertical displacement that a parcel initially at height z (in layer 2) undergoes as the CFA passes overhead, by evaluating the following integral:

$$\Delta z|_{\text{following a parcel}} = \int_0^t w_2'(\tau)\, d\tau|_{\text{following a parcel}}. \tag{10}$$

To evaluate this integral, we require an expression for w_2' following a parcel, but (9) is valid only at a fixed location, because it contains a local derivative of p'. Also, it is desirable that the final expression be cast in terms of pressure information that is available from a barograph at a fixed location. We start by defining the ''perturbation barogram'' as a function of time only, denoted by $B(t)$. Here, $B(t)$ is the barogram trace of p' at a fixed location, which can be obtained by subtracting the background linear tendency from the barogram trace of the total pressure. Assuming the p' pattern is a fixed structure moving at speed S, the pressure perturbation at any time and location can be expressed as $p'(x, t) = B(t - x/S)$, and the local tendency of p' at any time and x location can be expressed as $\partial p'(x, t)/\partial t = \dot{B}(t - x/S)$, where $\dot{B}$ is the first time derivative of B. The x position of a low-level parcel, which is assumed to move with the low-level background wind $\overline{u}$, obeys $x = x_0 + \overline{u}t$. Therefore, the value of the *local* tendency of the pressure perturbation *following a parcel* is given by

$$\left.\frac{\partial p'}{\partial t}\right|_{\text{following a parcel}} = \dot{B}\left(\left[1 - \frac{\overline{u}}{S}\right]t - \frac{x_0}{S}\right). \tag{11}$$

Combination of (9), (10), and (11) leads to the following integral:

$$\Delta z|_{\text{following a parcel}} = \int_0^t \frac{[z_t + A(z - z_t)]}{\rho S[S - \overline{u}(0)]}\dot{B}\left(\left[1 - \frac{\overline{u}}{S}\right]\tau - \frac{x_0}{S}\right) d\tau. \tag{12}$$

This integral can be solved by making the variable substitution $\chi = [1 - (\overline{u}/S)]\,\tau - (x_0/S)$ and $d\chi = [1 - (\overline{u}/S)]\,d\tau$, and by assuming that vertical excursions from the initial height are small relative to that initial height (i.e., that z can be treated as a constant inside the integral). The final expression is

$$\Delta z|_{\text{following a parcel}} = \frac{[z_t + A(z - z_t)]}{\rho[S - \overline{u}(0)][S - \overline{u}(z)]}B\left(\left[1 - \frac{\overline{u}}{S}\right]t - \frac{x_0}{S}\right). \tag{13}$$

Thus, (7), (8), (9), and (13) can be used to quantitatively estimate the convergence and vertical velocity as a function of time above a fixed barograph, as well as the net vertical ascent of a low-level air parcel traveling with the background wind over the barograph.

3. Two observed cases

Two warm occlusions were chosen that contained a CFA and/or a prefrontal surge, the passages of which were associated with local changes in the surface pressure that could be tracked through a surface observing

network. The structures of these occlusions were well documented by serial radiosondes, Doppler radar, and aircraft data during the Pacific Northwest CYCLES field project (Hobbs 1978).

Figure 3a shows the vertical structure of one of these warm occlusions during the passage of a CFA. This case, which occurred on 10 January 1976, was described by Hobbs and Locatelli (1978). A corresponding barogram for this case is shown in Fig. 3b. The perturbation barogram was constructed as follows. First, the average diurnal pressure tendency reported by Mass et al. (1991) for the Seattle–Tacoma International Airport was subtracted from the barogram trace, because this tendency is unrelated to any synoptic or mesoscale features. The trace was then enlarged for the time period of the CFA, and a 1-h time window associated with the passage of the CFA was selected. Care was taken to define the time $t = 0$ at a point where the pressure tendency was representative of the long-term pre-CFA tendency, but also as close as possible to the first noticeable signature of the CFA. Therefore, in each trace, the background pressure $\overline{p}$ is defined by a line tangent to the total pressure trace at $t = 0$, and the perturbation pressure p' is the difference between the actual pressure trace and the tangent line. This definition ensures that both p' and $\partial p'/\partial t$ are zero at $t = 0$. The perturbation barogram is shown in Fig. 3c.

The convergence for this case was estimated from the perturbation pressure trace, using (8) and the values of the case-dependent parameters shown in Table 2. The dashed curve in Fig. 3c shows the convergence thus obtained, for layer 2. The maximum convergence was approximately 0.7×10^{-4} s^{-1} at around 15 min. The maximum vertical velocity produced by the passage of the CFA was estimated at 7 cm s^{-1} by applying (9), and the vertical displacement after 1 h was estimated at 213 m by applying (13).

The second case considered here was a warm occlusion (described by Matejka 1980), which occurred on 7 January 1975 and contained both a prefrontal surge and a CFA. This case was analyzed in a similar way to the case described above. The results are shown in Fig. 4, where the prefrontal surge is labeled as feature A and the CFA as feature B. Maximum vertical velocities for a parcel at 1 km were estimated at 20 and 16 cm s^{-1}, respectively. Feature A produced a substantial vertical displacement estimated at 612 m after 1 h, for a parcel initially at 1 km. However, the pressure trace for feature B (Fig. 4d) contained two changes of opposite sign in pressure tendency, separated by only 20 min. Therefore, the large initial convergence in feature B was quickly reduced and became divergence. This resulted in a modest vertical displacement estimated at 184 m.

4. Results from a mesoscale model simulation

The Penn State–NCAR MM5 mesoscale model (Grell et al. 1994) was used to simulate a cyclonic storm that

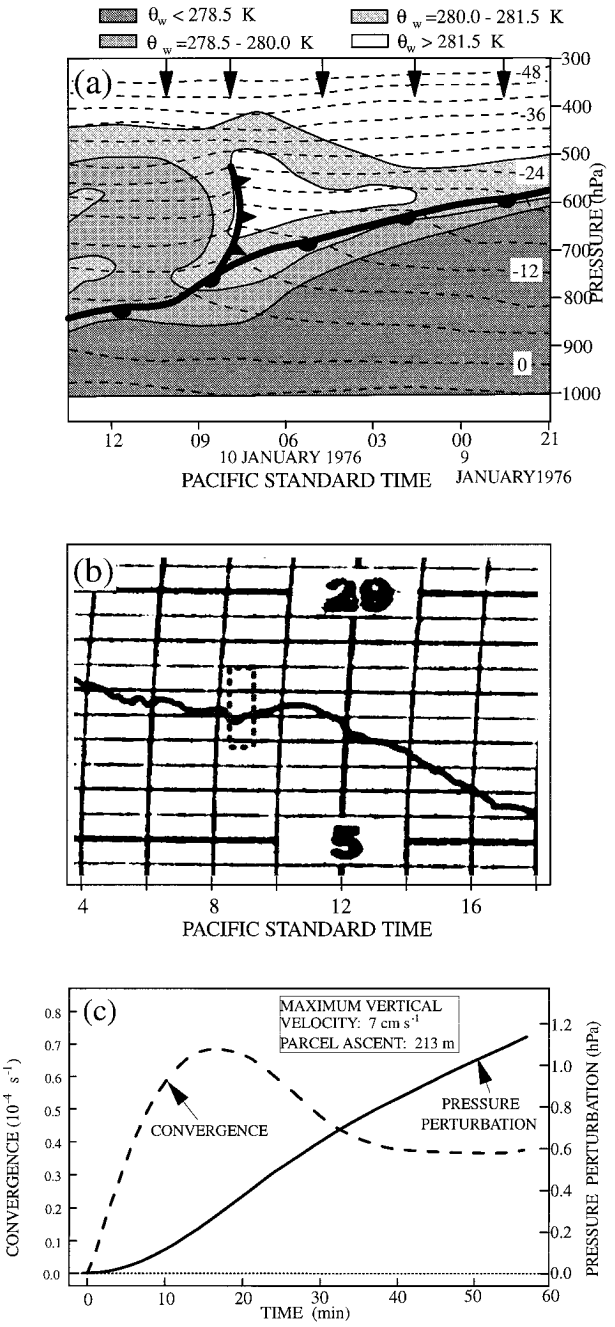

FIG. 3. (a) Vertical cross section through a cold front aloft as it passed over Seattle on 9–10 January 1976. The dashed lines are isotherms, shown every 4°C and labeled every 12°C. Values of wet-bulb potential temperature θ_w are indicated by the shading. Heavy vertical arrows indicate times of radiosonde launches. Adapted from Hobbs and Locatelli (1978). (b) Barogram for Seattle on 10 January 1976. The dashed box indicates the region of the barogram enlarged in (c), which encompasses the time of the passage of the cold front aloft shown in (a). Each vertical division is 1.7 hPa. (c) Enlarged view of the segment of the barogram within the dotted box in (b), showing the perturbation pressure and the resulting CFA-induced surface convergence.

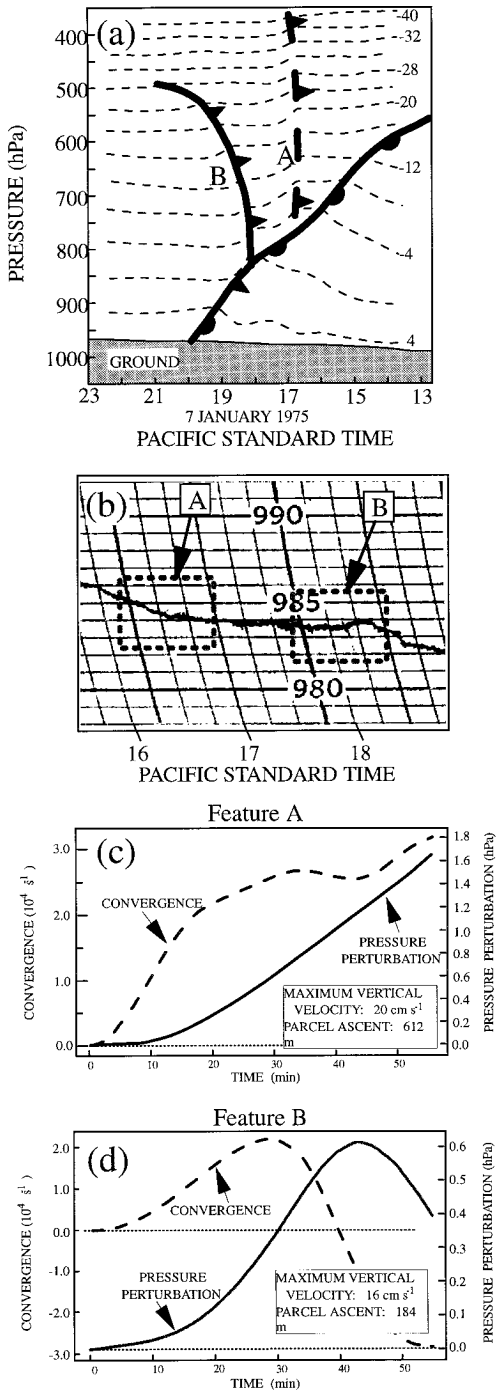

FIG. 4. (a) Vertical cross section through a prefrontal surge (marked by A) and a cold front aloft (marked by B) as they passed over Seattle on 7 January 1975. The dashed lines are isotherms, shown every 4°C and labeled every 8°C. Adapted from Matejka (1980). (b) Barogram for Seattle on 7 January 1975. The dashed box labeled A indicates the region of the barogram trace enlarged in (c), which encompasses the time of the passage of the prefrontal surge, and the dashed box labeled B indicates the region of the barogram trace enlarged in (d), which encompasses the time of the passage of the cold front aloft. Each vertical division is 1.0 hPa. (c) Enlarged view of the segment of the barogram within the dotted box labeled A in (b), showing the perturbation pressure and the resulting CFA-induced surface convergence. (d) Enlarged view of the segment of the barogram within the box labeled B in (b), showing the perturbation pressure and the resulting CFA-induced surface convergence.

occurred in the central United States on 9 March 1992 during the Stormscale Operational and Research Meteorology Fronts Experiment Systems Test (STORM-FEST). The MM5 model is a nonhydrostatic, primitive equation model that uses the terrain-following sigma vertical coordinate, and a rectangular grid on a conformal map projection. Specific physical parameterizations include the high-resolution PBL scheme developed by Blackadar (1979), the Kain–Fritsch (1990) cumulus parameterization, and the explicit cloud microphysical scheme (including separate treatment of cloud water, rain, cloud ice, and snow) implemented by Reisner et al. (1993).

This model simulation was run on a domain with 8.3-km resolution, covering the region of northern Texas, Oklahoma, Kansas, southern Nebraska, and western Missouri. The model was initialized at 0000 UTC 9 March 1992. Initial and boundary conditions were interpolated from the output of a lower-resolution model run that was initialized 12 h earlier. That earlier model run was initialized from objective analyses of standard and special STORM-FEST observations.

During the course of this storm, a CFA overran a stationary arctic front in the central United States north of Kansas, as shown by the observational analysis in Fig. 5 [see also Figs. 2a, 3a, and 9 in Wang et al. (1995)]. Figure 6 shows a surface plot of model-simulated convergence and wind vectors valid at 0530 UTC 9 March 1992, along with analyses of the surface arctic front, the CFA, and the lee trough. Two regions of convergence are labeled C1 and C2. Feature C1 corresponds to the surface position of the southeastward advancing arctic front, and feature C2 corresponds to the surface signature of the northeastward moving CFA. South of feature C1, there are also two north–south-oriented convergence features. The more eastward one is also associated with the CFA, as the CFA (in the model simulation) turns sharply southward across the arctic front into Kansas. The second north–south line of convergence in Kansas is due to a surface lee trough.

Figure 7 shows a cross section along the line *AA′* in Fig. 6, which cuts approximately perpendicularly through both the surface arctic front and the CFA. The two panels correspond to time periods 0330 UTC and 0530 UTC 9 March 1992, respectively. Shown on the cross sections are potential temperature, wind vectors within the plane of the cross section, and convergence. The arctic front is clearly seen as an abrupt transition in the low-level potential temperature gradient at approximately 60 km from the left edge of the cross section shown at both times. The arctic front was nearly stationary at this time and location. Above the arctic air

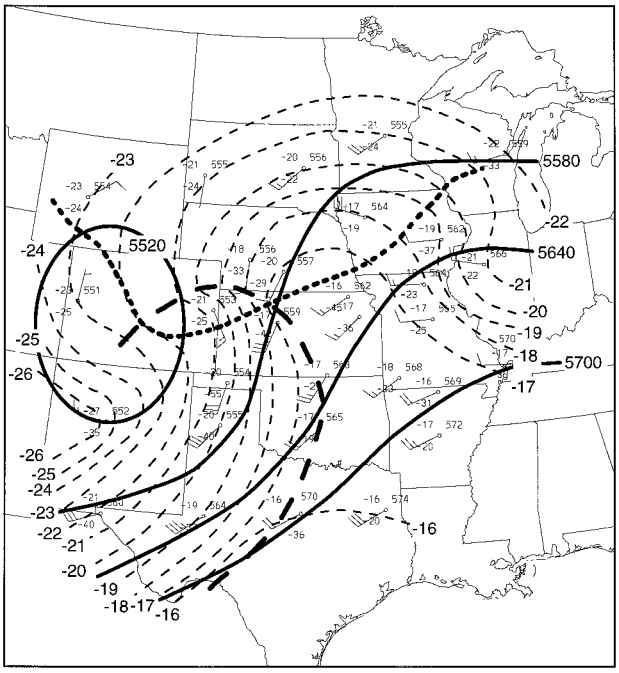

FIG. 5. The 500-hPa analysis at 0300 UTC 9 March 1992. Solid lines are geopotential height labeled in meters. Dashed lines are isotherms labeled in degrees Celsius and contoured every 1°C. Wind speeds are indicated by short barbs (5 m s^{-1}) and long barbs (10 m s^{-1}). Station data are plotted in the standard upper-level station model format. The heavy dashed line is the position of the CFA at 500 hPa. The heavy dotted line is the position of the surface arctic front.

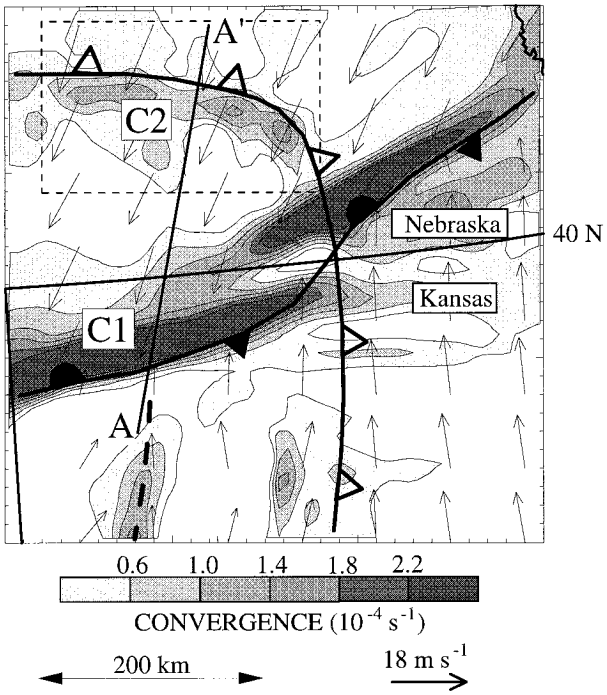

FIG. 6. Surface map of horizontal convergence (shaded, with values labeled on gray scale) and horizontal wind (arrows) from an MM5 mesoscale model simulation valid at 0530 UTC 9 March 1992. Subjectively analyzed features (based on model output) include the surface arctic front (shown as a stationary front), the CFA (open triangles), and the surface lee trough (heavy dashed line). Regions of convergence marked C1 and C2 are described in text. Line *AA′* indicates the location of the cross section shown in Fig. 7. The dashed rectangle indicates the subdomain that is shown in Fig. 8.

mass, the CFA was the leading edge of a cold air mass aloft, which impinged on the warmer air ahead of it. Three regions of convergence are labeled in Fig. 7. The convergence associated with the leading edge of the stationary arctic front is marked C1 and the CFA-induced surface convergence is marked C2, corresponding to the like-named features in Fig. 6. Also, a region of midlevel convergence associated with the CFA is marked C3. A slightly enhanced vertical velocity associated with the CFA-induced surface convergence can be seen in the wind vectors.

The dashed box in Fig. 6 is a smaller region for which surface convergence and wind vectors, sea level pressure, and horizontal Laplacian of pressure at the surface are shown in Figs. 8a, 8b, and 8c, respectively. Comparing the wind vectors in Fig. 8a with the pressure pattern in Fig. 8b, we see that north of the region of CFA-induced surface convergence and the associated pressure pattern, the winds cross the isobars at an angle of about 40°. South of this region, where the pressure pattern associated with the CFA has already passed, the wind direction has hardly changed, but the wind speed has slightly decreased as shown by the slight decrease in the length of the wind vectors. This observation indicates that uniform flow (presumably near geotriptic balance) existed prior to the passage of the CFA, and air parcels that subsequently were overtaken by the moving pressure pattern associated with the CFA did not have time to attain geotriptic balance within the region of changing horizontal pressure gradient; instead they were simply decelerated. We have marked the axis of maximum surface convergence associated with the CFA with a heavy dashed line in Fig. 8; the Laplacian of pressure changes sign from positive to negative along this axis. This is consistent with the relationship between convergence and the pressure Laplacian implied by (4), namely, that if the Laplacian of pressure is positive, the CFA-induced surface convergence at a fixed point will continue to increase with time until the Laplacian of pressure changes sign.

To study in more detail the CFA-induced surface convergence simulated by the MM5 model, we now look at smaller-scale cross sections along the line marked *BB′* in Fig. 8. Shown in Fig. 9a is the horizontal component of the wind along the cross section relative to the speed of the CFA. Two important features can be seen: the strong shear layer associated with the arctic front, and the leading edge of the moving cold air aloft as indicated by the zero contour line. The positions of the arctic front and the CFA are taken from Fig. 7b.

It is instructive to examine how the horizontal density structures at various levels in the atmosphere contribute

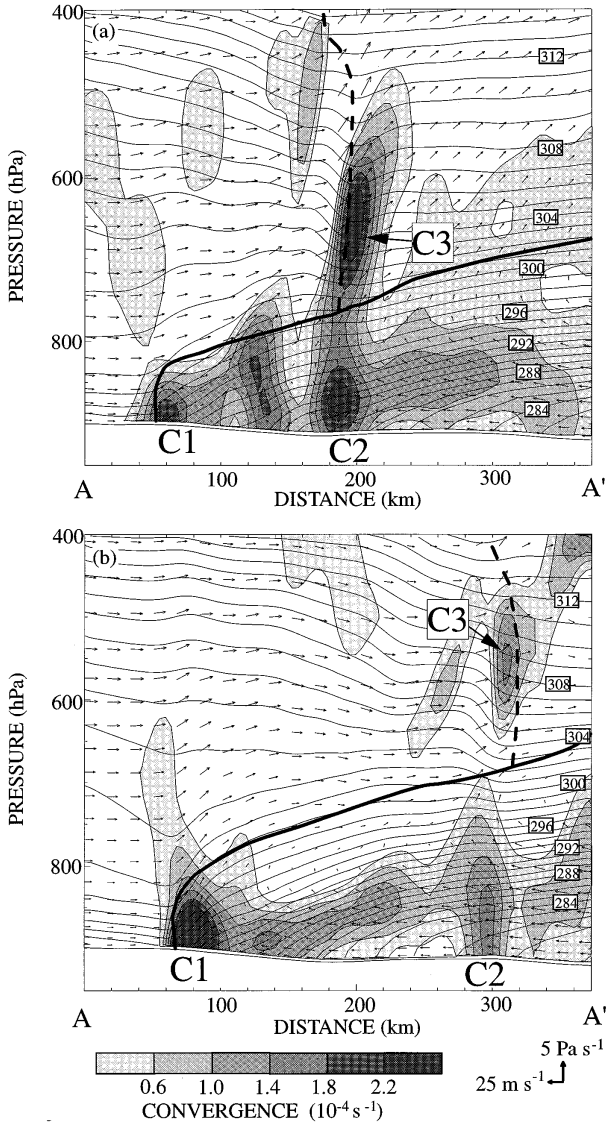

FIG. 7. (a) Vertical cross section from an MM5 mesoscale model simulation valid at 0330 UTC 9 March 1992 along line *AA′* in Fig. 6. The solid lines are contours of potential temperature θ, shown every 1 K and labeled every 4 K. Arrows are wind vectors in the plane of the cross section. Horizontal convergence is shown by the shading. The heavy solid line indicates the arctic front, and the heavy dashed line the cold front aloft. See text for an explanation of the regions of convergence labeled C1, C2, and C3. (b) As for (a) but for 0530 UTC 9 March 1992.

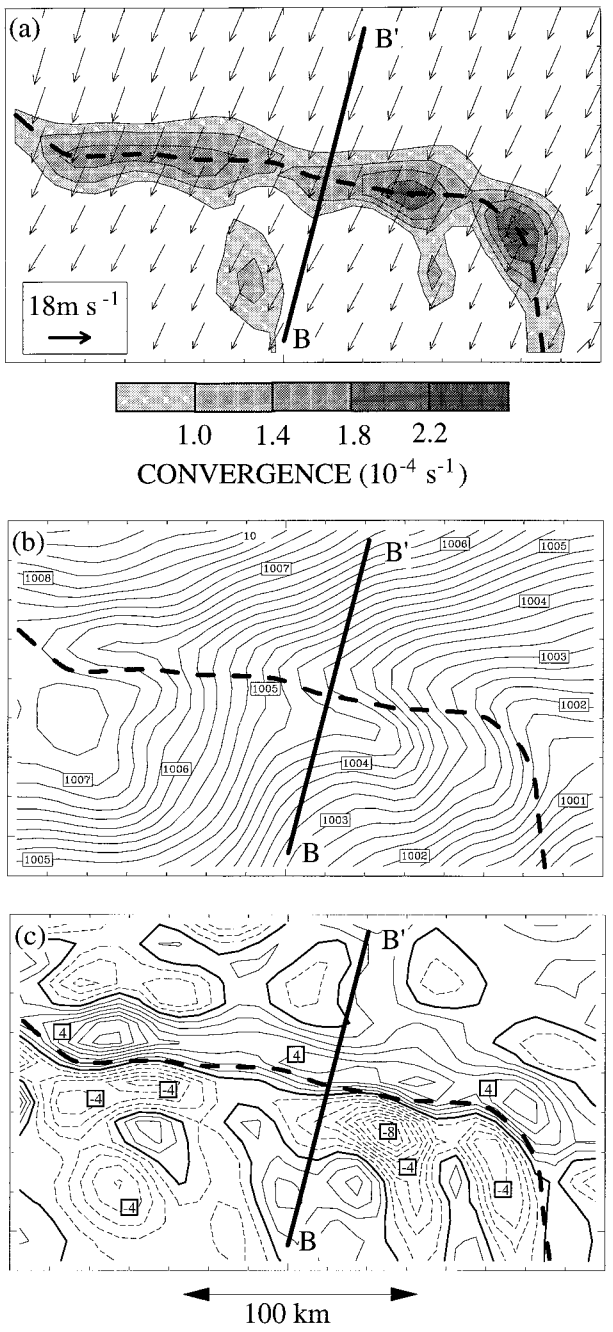

FIG. 8. (a) Surface map of horizontal convergence (shading) and horizontal wind vectors (arrows) from an MM5 mesoscale model simulation valid at 0530 UTC 9 March 1992 for the region located within the dashed box shown in Fig. 6. Vector scale is shown at lower left, and convergence values are shown on the labeled gray scale. The heavy dashed line marks the axis of maximum convergence. (b) As for (a) but solid lines are isobars of sea level pressure, contoured every 0.25 hPa and labeled every 1 hPa. (c) As for (a) but the solid lines (dashed lines) are positive values (negative values) of the horizontal Laplacian of pressure at the surface, contoured every 1×10^{-7} Pa m^{-2} and labeled every 4×10^{-7} Pa m^{-2}. The zero contour of the Laplacian is indicated by the heavier contour lines. Line *BB′* indicates the location of the cross section shown in Fig. 9.

to the horizontal Laplacian of pressure at the surface. The contribution to the horizontal Laplacian of pressure at the surface, per unit thickness of layers aloft, is $g\nabla_h^2\rho$, or $\rho^{-1}\nabla_h^2\rho$ per unit pressure thickness of layers aloft. This quantity is contoured in Fig. 9b. Two columns of large positive and negative contributions are located to the left of the CFA position, extending from around 850 to around 550 hPa, which produce the pattern of the Laplacian shown in Fig. 8c associated with the CFA-induced surface convergence. It can be seen that the

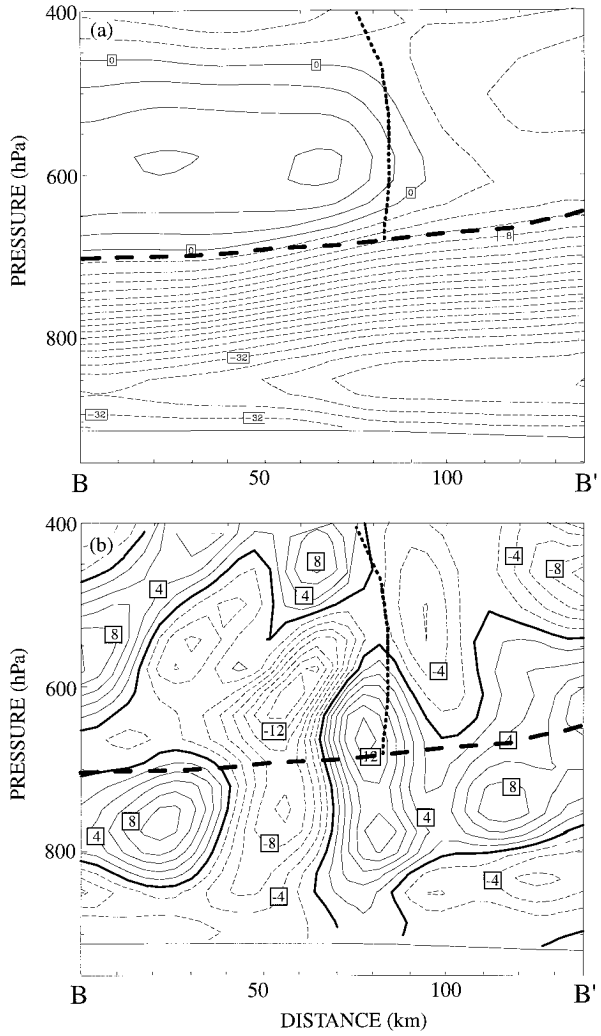

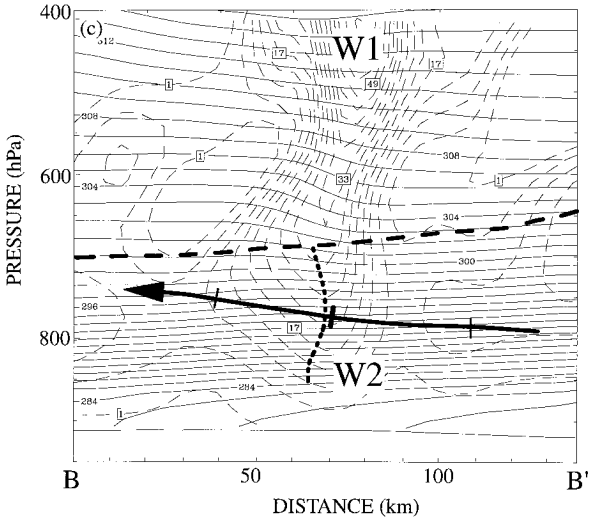

FIG. 9. (a) Vertical cross section along line *BB′* in Fig. 8 of the horizontal wind component (contoured every 2 m s^{-1}) in the plane of the cross section, relative to the speed of the CFA. The winds are taken from the mesoscale model simulation valid at 0530 UTC 9 March 1992. Solid (dashed) lines are contours of relative wind moving left to right (right to left) [in the same (opposing) direction as the motion of the cold front aloft]. The heavy dashed line marks the arctic front and the heavy dotted line the cold front aloft. (b) As for (a) but the solid lines (dashed lines) are positive values (negative values) of the contribution (per hectopascal layer thickness) of the density Laplacian at each pressure level to the horizontal Laplacian of pressure at the surface. Values are contoured every 1×10^{-7} Pa m^{-2} and labeled every 4×10^{-7} Pa m^{-2}. The zero contours of the contribution to the Laplacian are indicated by the heavier solid lines. (c) As for (a) but dashed lines are contours of upward vertical air velocity shown ever 4 cm s^{-1} and labeled every 16 cm s^{-1}, and solid lines are contours of potential temperature, shown every 1 K and labeled every 4 K. See text for an explanation of the trajectory (heavy arrow) and vertical velocity regions labeled W1 and W2.

main positive contribution comes from the baroclinic zone directly behind the CFA, immediately above the arctic front. However, there are also substantial contributions in the columns below the arctic front. This secondary effect is due to the lifting of air parcels in the boundary layer beneath the CFA. This lifting produces a temperature pattern at low levels that is in phase with the temperature pattern at the level of the CFA.

In Fig. 9c, vertical air velocity and potential temperature θ are plotted for cross section *BB′*. Two regions of relatively high vertical velocity are present. The first, marked W1, is at midlevels and immediately precedes the CFA. The second, marked W2, is associated with the CFA-induced surface convergence. The dividing line between the columns of positive and negative contributions to the horizontal Laplacian of pressure on the surface below the arctic front is marked by the heavy dotted line in Fig. 9c. Figure 9a shows that, relative to the moving CFA and the associated vertical velocity pattern, air parcels move from right to left in the cross section below the arctic front. The arrow in Fig. 9c depicts a trajectory of an air parcel that is overtaken by the moving pattern of vertical velocity. It was calculated from half-hourly velocity fields from the model output using three-dimensional winds linearly interpolated in time to 10-min time steps. The displayed parcel path on the cross section consists of the projection of the trajectory onto the plane of the cross section. The hatch marks show half-hour intervals along the trajectory for 0500, 0530, and 0600 UTC 9 March 1992, with the middle (heavy) hatch mark corresponding to the time of the plotted fields in the figure. A corresponding perturbation can be seen in the potential temperature field, but the trajectory does not necessarily follow an isentrope, because latent heating is occurring along the trajectory, and the situation is not steady state. The displacement of the θ contours also shows the secondary effect described above, namely, a low-level potential temperature pattern that is in phase with the temperature pattern at the level of the CFA. Since this secondary potential temperature pattern moves with the CFA, the

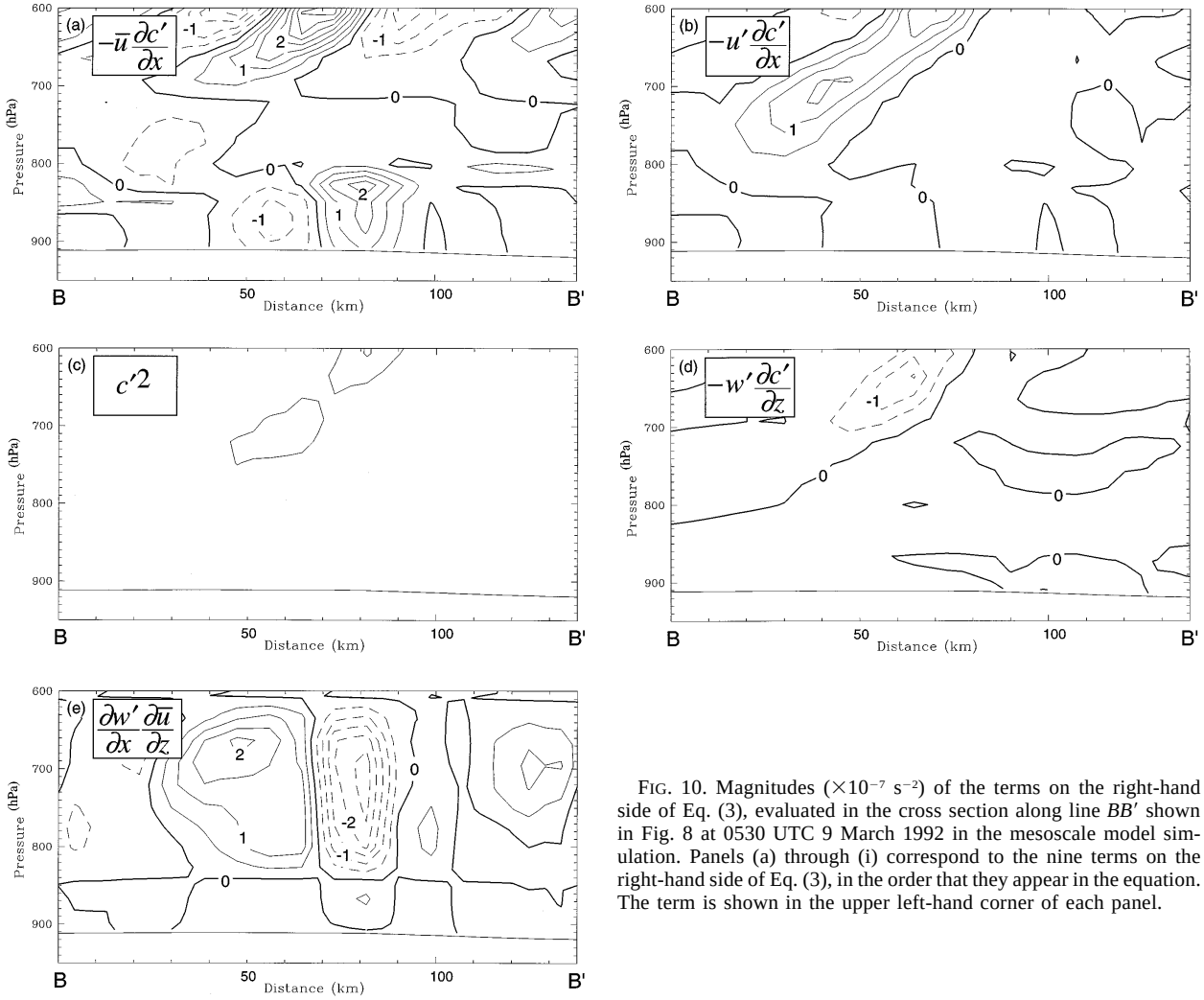

FIG. 10. Magnitudes ($\times 10^{-7}$ s^{-2}) of the terms on the right-hand side of Eq. (3), evaluated in the cross section along line *BB′* shown in Fig. 8 at 0530 UTC 9 March 1992 in the mesoscale model simulation. Panels (a) through (i) correspond to the nine terms on the right-hand side of Eq. (3), in the order that they appear in the equation. The term is shown in the upper left-hand corner of each panel.

pressure changes it produces contribute to the moving pressure pattern induced by the CFA at the surface.

As a check on the scale analysis performed in section 2, the terms on the right-hand side of (3) were evaluated from model output for the 9 March 1992 case, at 0530 UTC. The x axis was taken along the cross section *BB′* shown in Fig. 8. The nine different terms, in the order that they appear in (3), are shown in Figs. 10a–i, respectively. It can be seen that within the lowest 1 km of the cross section (or approximately between 810 and 910 hPa), panels (a), (e), and (g) show values of 1–3 s^{-2} $\times$ 10^{-7}. These panels correspond to the terms $-\overline{u}\partial c'/\partial x$, $(\partial w'/\partial x)(\partial \overline{u}/\partial z)$, and $\rho^{-1}\partial^2 p'/\partial x^2$, which are the same terms that were found to be significant in the scale analysis. Panels (b), (c), (d), (f), (h), and (i) confirm that the terms in the lowest 1 km neglected in the scale analysis are indeed small relative to the terms that are retained.

A surface barogram of total pressure (not shown) and pressure perturbation (Fig. 11) at a location in the middle of cross section *BB′* was created from model output. Also shown in the barogram is an estimated trace of convergence [calculated by applying (8) to the layer below 700 m], the maximum of which is 1.8×10^{-4} s^{-1}. Figure 11 also shows estimates of the maximum vertical velocity at 1 km [calculated from (9)] and the ascent over 1 h of a parcel, initially at 1 km, over which the CFA passes [calculated from (13)], which are 13 cm s^{-1} and 118 m, respectively. For comparison, the actual values of these estimated quantities can be ascertained from previous figures. Figure 7 shows that the convergence in feature C2 (the CFA-induced surface convergence) is around 2 $\times$ 10^{-4} s^{-1}. Figure 9c shows the maximum vertical velocity at 1 km (or approximately 810 hPa) is 17 cm s^{-1} and the vertical deviation of the trajectory during the 1-h period is approximately 220 m. These comparisons show that, despite the many assumptions made in the analysis in section 2, the equations that were derived provide useful estimates of the convergence and ascent induced by the moving surface pressure signature associated with a CFA passage.

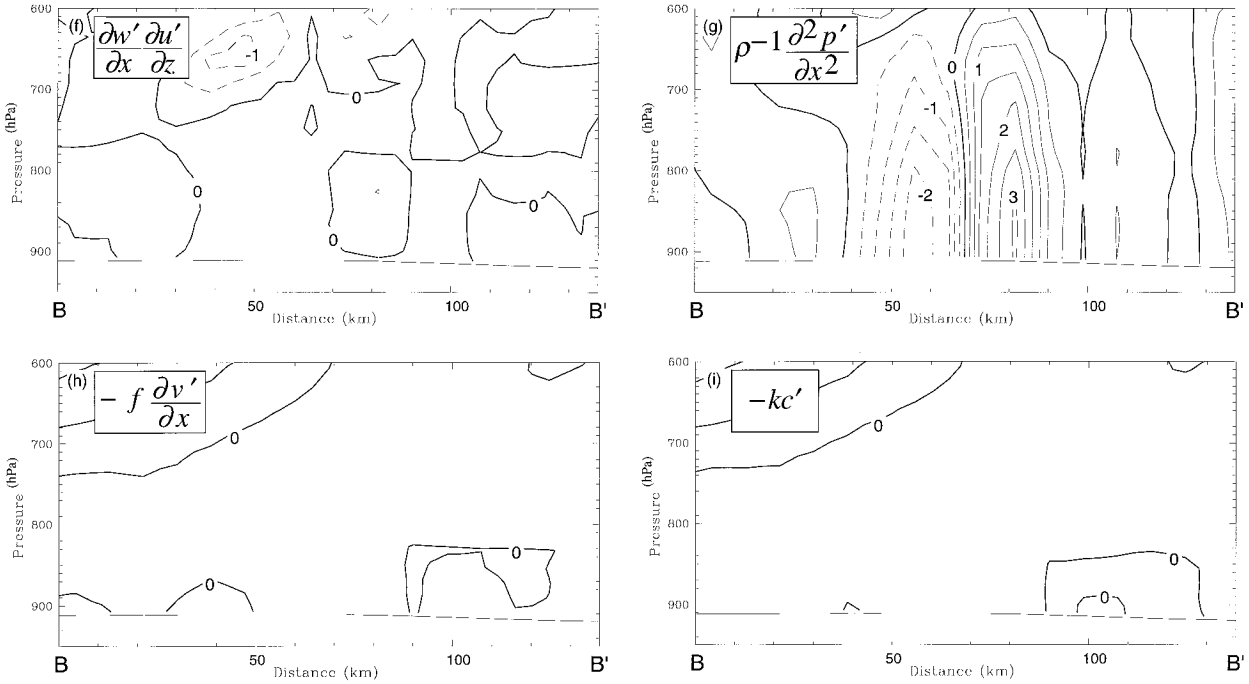

FIG. 10. (*Continued*)

5. Discussion and conclusions

We have shown that the movement of a CFA or a prefrontal surge aloft, and the moving horizontal pressure gradient that these features give rise to at the surface, produces surface convergence and upward air motion in the boundary layer. The response at low levels is similar to that of a ducted (or partially ducted) mesoscale gravity wave, such as those studied by Powers and Reed (1993), in that it is a propagating feature with similar phase relationships between pressure perturbation, vertical velocity, and temperature. However, the motion of the pressure disturbance at the surface is clearly set by the speed of the CFA. It is possible that this phenomenon can be described in terms of a forced gravity wave that is locked to the pressure perturbation associated with the advancement of the CFA over a stable warm front.

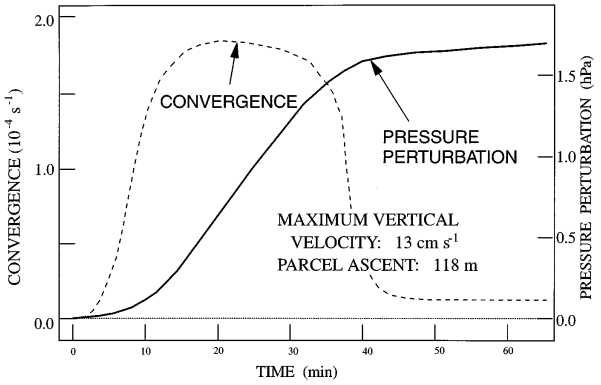

FIG. 11. Model-simulated surface pressure perturbation and estimated convergence versus time at the midpoint of cross section *BB′* shown in Fig. 8. The point $t = 0$ corresponds to 0500 UTC 9 March 1992.

The ascent associated with the surface convergence produced by the CFA feeds back to the moving pressure pattern through adiabatic cooling; condensation and precipitation in the column complicate the phenomenon. However, all such processes and feedbacks are reflected in the surface pressure pattern. As such, the forces on an air parcel at the surface, calculated using barogram pressure traces (as in section 3), will result in an accurate estimate of the CFA-induced surface convergence provided the surface pressure pattern associated with the moving feature aloft is essentially two-dimensional, structurally invariant, and the horizontal pressure gradient above the surface is not significantly different from the horizontal pressure gradient at the surface. A model simulation of the CFA-induced surface convergence (see section 4) has shown that, in at least one case, convergence did not vary significantly with height in the lowest 1 km.

This study has also shown that, for timescales of 1 h or less, the form of the linear divergence equation developed here is a useful tool for estimating the convergence and vertical air velocity associated with changes in horizontal pressure gradient (or tendency). This is because, unlike the quasigeostrophic isallobaric wind equation, the linear divergence equation does not require the assumption of geostrophic balance. Rather, it relates convergence to the *imbalance* of forces that can develop during short time periods. Mesoscale model output showed that (4) and its related equations [(8), (9), and

(13)] can be used to estimate the convergence, vertical velocity, and vertical displacement of low-level air parcels that experienced the pressure tendency change associated with the passage of a CFA.

Bluestein (1993, 450) has discussed the properties of air masses associated with convective precipitation and presents soundings typical of these air masses. Bluestein's ''Miller type 1'' (Miller 1972), sounding requires 50–100 hPa of lift between 900 and 700 hPa to trigger severe convection. The sounding used in the modeling study of Rotunno et al. (1988), which they describe as ''broadly typical of the environment of midlatitude squall lines,'' needs less than 50 hPa of lift between 900 and 700 hPa to trigger convection. Stratiform precipitation requires vertical velocities on the order of tens of centimeters per second. The results of this study show that surface convergence induced by a CFA can lead to vertical velocities on the order of tens of centimeters per second, and displacements of air parcels on the order of tens of hectopascals. Therefore, surface convergence produced by a CFA may be a significant factor in the release of convective instability within the unstably stratified warm-occluded-like structure of the type depicted in the STORM conceptual model. Of course, other ascent-forcing mechanisms, such as quasigeostrophic forcing and gravity waves propagating downstream from the Rocky Mountains, may also release convective instability.

Acknowledgments. This research was supported by Grant ATM-9106235 from the Atmospheric Research Division of the National Science Foundation.

REFERENCES

Blackadar, A. K., 1979: High resolution models of the planetary boundary layer. *Advances in Environmental Science and Engineering*, Vol. 1, J. B. Pffaffin and E. N. Zeigler, Eds., Gordon and Breach, 50–85.

Bluestein, H. B., 1993: *Synoptic-Dynamic Meteorology in Midlatitudes.* Vol. II, *Observations and Theory of Weather Systems,* Oxford University Press, 594 pp.

Galloway, J. L., 1958: The three-front model: Its philosophy, nature, construction and use. *Weather,* **13,** 3–10.

Gill, A. E., 1982: *Atmosphere-Ocean Dynamics.* Academic Press, 662 pp.

Grell, G. A., J. Dudhia, and D. R. Stauffer, 1994: A description of the Fifth Generation Penn State/NCAR Mesoscale Model (MM5). NCAR Tech. Note NCAR/TN-398+STR, 121 pp. [Available from National Center for Atmospheric Research, Boulder, CO 80301-3000.]

Hobbs, P. V., 1978: Organization and structure of clouds and precipitation on the mesoscale and microscale in cyclonic storms. *Rev. Geophys. Space Phys.,* **16,** 741–755.

——, and J. D. Locatelli, 1978: Rainbands, precipitation cores and generating cells in a cyclonic storm. *J. Atmos. Sci.,* **35,** 230–241.

——, ——, and J. E. Martin, 1996: A new conceptual model for cyclones generated in the lee of the Rocky Mountains. *Bull. Amer. Meteor. Soc.,* **77,** 1169–1178.

Holton, J. R., 1992: *An Introduction to Dynamic Meteorology.* 2d ed. Academic Press, 511 pp.

Holzman, B., 1936: Synoptic determination and forecasting significance of cold fronts. *Mon. Wea. Rev.,* **64,** 400–413.

Johnson, W. B., Jr., 1966: The ''geotriptic'' wind. *Bull. Amer. Meteor. Soc.,* **47,** 982.

Kain, J. S., and J. M. Fritsch, 1990: A one-dimensional entrainment/detrainment plume model and its application in convective parameterization. *J. Atmos. Sci.,* **47,** 2784–2802.

Kreitzberg, C. W., and H. A. Brown, 1970: Mesoscale weather systems within an occlusion. *J. Appl. Meteor.,* **9,** 417–432.

Lichtblau, S., 1936: Upper cold fronts in North America. *Mon. Wea. Rev.,* **64,** 414–425.

Locatelli, J.D., P. V. Hobbs, and J. A. Werth, 1982: Mesoscale structures of vortices in polar air streams. *Mon. Wea. Rev.,* **110,** 1417–1433.

——, J. E. Martin, J. A. Castle, and P. V. Hobbs, 1995: Structure and evolution of winter cyclones in the central United States and their effects on the distribution of precipitation. Part III: The development of a squall line associated with weak cold-frontogenesis aloft. *Mon. Wea. Rev.,* **123,** 2641–2662.

Martin, J. E., J. D. Locatelli, P. V. Hobbs, P.-Y. Wang, and J. A. Castle, 1995: Structure and evolution of winter cyclones in the central United States and their effects on the distribution of precipitation. Part I: A synoptic-scale rainband associated with a dryline and lee trough. *Mon. Wea. Rev.,* **123,** 241–264.

Mass, C. F., W. J. Steenburgh, and D. M. Schultz, 1991: Diurnal surface-pressure variations over the continental United States and the influence of sea level reduction. *Mon. Wea. Rev.,* **119,** 2814–2830.

Matejka, T. J., 1980: Mesoscale organization of cloud processes in extratropical cyclones. Ph.D. thesis, University of Washington, 361 pp. [Available from University Microfilms, 300 Zeeb Road, Ann Arbor, MI 48106.]

——, R. A. Houze Jr., and P. V. Hobbs, 1980: Microphysics and dynamics of clouds associated with mesoscale rainbands in extratropical cyclones. *Quart. J. Roy. Meteor. Soc.,* **106,** 29–56.

Matkovskii, B. M., and N. P. Shakina, 1982: Mesoscale structure of an occluded front over the center of the European USSR from special measurements. *Meteor. Gidrol.,* **1,** 24–33.

Miller, R. C., 1972: Notes on analysis and severe storms forecasting procedures of the Air Force Global Weather Central. Tech. Rep. 200 (rev.) Air Weather Service, 181 pp. [Available from NTIS, 5285 Port Royal Road, Springfield VA 22161; NTIS AD 744042.]

Powers, J. G., and R. J. Reed, 1993: Numerical simulation of the large-amplitude mesoscale gravity-wave event of 15 December 1987 in the central United States. *Mon. Wea. Rev.,* **121,** 2285–2308.

Reisner, J., R. T. Bruintjes, and R. M. Rasmussen, 1993: Preliminary comparisons between MM5 NCAR/Penn State model generated icing forecasts and observations. Preprints, *Fifth Int. Conf. on Aviation Weather Systems,* Vienna, VA, Amer. Meteor. Soc., 65–69.

Rotunno, R., J. B. Klemp, and M. L. Weisman, 1988: A theory for strong, long-lived squall lines. *J. Atmos. Sci.,* **45,** 463–485.

Showalter, A. K., and J. R. Fulks, 1943: Preliminary report on tornadoes. U.S. Department of Commerce, Weather Bureau, War Advisory Council on Meteorology, Restricted Rep. 1110, 162 pp. [Available from NOAA Central Library, SSMC3 7th Floor, 1315 East–West Highway, Silver Spring, MD 20910.]

Wang, P. Y., J. E. Martin, J. D. Locatelli, and P. V. Hobbs, 1995: Structure and evolution of winter cyclones in the central United States and their effects on the distribution of precipitation. Part II: Arctic fronts. *Mon. Wea. Rev.,* **123,** 1328–1344.

Wexler, H., 1935: Analysis of a warm-front-type occlusion. *Mon. Wea. Rev.,* **63,** 213–221.

Williams, D. T., 1953: Pressure wave observations in the central Midwest, 1952. *Mon. Wea. Rev.,* **81,** 278–289.